



Effects of novel polymer-type shrinkage-reducing admixture on early age autogenous deformation of cement pastes



Wenqiang Zuo^{a,b,c}, Pan Feng^{a,*}, Peihua Zhong^{a,b,c}, Qian Tian^{b,c}, Nanxiao Gao^{b,c},
Yujiang Wang^{a,b,c}, Cheng Yu^{b,c}, Changwen Miao^{a,b,c}

^a School of Materials Science and Engineering, Southeast University, Nanjing 211189, China

^b Jiangsu Research Institute of Building Science Co., Ltd, Nanjing 210008, China

^c State Key Laboratory of High Performance Civil Engineering Materials, Nanjing 210008, China

ARTICLE INFO

Keywords:

Admixture (D)
Shrinkage (C)
Pore solution (B)
Hydration (A)
Hydration products (B)

ABSTRACT

This study aims to investigate the autogenous shrinkage-reducing mechanisms of the novel polymer-type shrinkage-reducing admixture (SRA) with water-reducing function. For comparison, the traditional polyether-type SRA was also used. The development of autogenous deformation, hydration rate, internal relative humidity (RH), electrical resistivity, ions and SRAs concentration in pore solutions and crystal content of cement pastes were comprehensively investigated. Unlike the polyether-type SRA mixture which has an expansion period at early age, a relatively slow and monotonous evolution of shrinkage was observed for the polymer-type SRA mixture. It is concluded that the delay and regulation effects on cement hydration of the novel SRA obviously influence the microstructure development and the evolutions of various performances of cement pastes comparing to the polyether-type SRA. Furthermore, both the self-desiccation status induced capillary pressure and the crystallization pressure induced expansion stress contribute to the shrinkage-reducing behaviors of SRAs on the autogenous deformation of the cement pastes.

1. Introduction

Shrinkage is a common phenomenon in modern concrete and if not handled properly, it may lead to serious problems such as cracking and failure of the structure. Especially in high-performance concrete, the low water-to-cement ratios can result in an obvious autogenous shrinkage during the hydration of cement even under sealed conditions [1–5]. In recent decades, numerous experimental studies have been done to investigate various properties of cement-based materials with the addition of SRA, such as autogenous and drying shrinkage [6–10], plastic shrinkage [11–13], mechanics and hydration behaviors [14–15] as well as the moisture evaporation and capillary suction [5,16] of cementitious materials, etc.

As a special type of organic chemical admixtures, SRA had been introduced to mitigate shrinkage and control crack of cement-based materials since 1980s [4]. And it is considered as one of the most effective methods to reduce the shrinkage of concrete especially the autogenous and drying shrinkage [5–10]. Although the shrinkage-reducing mechanism of SRA is still not fully understood, most studies, however, hold the view that by adding SRA into cementitious systems, the surface tension of the pore solution in capillary pores is significantly

lowered [4,8,10]. According to the Young-Laplace equation (Eq.(1)) and Kelvin equation (Eq.(2)), under sealed condition, after the formation of the solid microstructure, the lower surface tension in turn can reduce the capillary pressure and maintain the internal RH in a higher level [3,14]:

$$\sigma_{cap} = -2\gamma_{LV}\cos\theta/r \quad (1)$$

$$\ln(RH) = -V_m/RT \cdot 2\gamma_{LV}\cos\theta/r \quad (2)$$

where σ_{cap} is the capillary pressure (MPa), r is the menisci curvature radius (m), γ_{LV} is the surface tension of the pore solution (N/m), θ is the contact angle, V_m is the molar volume of the pore solutions (assumed to be water, 18.02 cm³/mol), R is the gas constant (8.314 J/kmol), and T is the absolute temperature (293.15 K). Therefore, the macroscopic shrinkage stress of cementitious materials drops under the condition of moisture consumption.

Besides, the addition of SRA can reduce the concentration of Na⁺ and K⁺ in the pore solutions, which decreases the concentration of the counterbalancing anion such as SO₄²⁻ and OH⁻ comparing to the plain mixture, in turn increase the concentration of Ca²⁺ (common ion effect) and the oversaturation of portlandite and ettringite [4], especially

* Corresponding author.

E-mail address: pan.feng@seu.edu.cn (P. Feng).

Table 1
Chemical and mineral composition of the cement.

Chemical composition (% by mass)							
SiO ₂	Al ₂ O ₃	CaO	MgO	Fe ₂ O ₃	SO ₃	NA ₂ O _{eq}	Ignition loss
21.08	4.29	62.68	1.55	3.94	2.55	0.48	2.31
Mineral composition (% by mass)							
C ₃ S	C ₂ S	C ₃ A	C ₄ AF				
52.50	21.40	6.40	13.10				

the crystallization of portlandite. Therefore, an early age expansion usually occurs which also plays an important role to compensate shrinkage stress partially [9,17–18].

Besides the investigations of the shrinkage-reducing mechanisms, recently, an increasing number of studies also focus on the development of new type of multifunctional chemical admixtures, among which the polymeric water-reducing type of SRA has been designed and investigated [19–21] which provides a vast space for the application of the concrete SRA. While possessing an excellent shrinkage-reducing effect on the cementitious materials, the novel type of water-reducing SRA also has a significant function of water-reducing which seems to be more economical and efficient. However, the specialized study on the mechanism of the novel type of SRA is seldom found [22].

In this paper, the impacts of a traditional polyether-type SRA (SRA1) and a novel polymer-type SRA (SRA2) on the early age autogenous deformation of cement pastes are investigated. The performance of mixtures with SRAs on autogenous deformation, hydration rate and dynamic elastic modulus were compared to the plain mixture. Finally, mechanisms of shrinkage reducing of different types of SRA at early age of cement pastes are revealed.

2. Materials, mix proportion and experimental procedures

2.1. Materials

Portland cement with strength grade of 52.5 MPa obtained from Xiao Yetian Cement Co., Ltd. (Jiangsu, China) was used. The apparent density of cement is 3060 kg/m³, and the chemical and mineral compositions are listed in Table 1, which are obtained by the X-ray fluorescence spectrometer and X-ray diffractometer, respectively.

The tap water was used. The polycarboxylate-type of water-reducing agent (SP) was used as admixture with the solid content of 10% and the water-reducing ratio at around 35%. Two types of SRAs with different molecular structure were used and their basic physicochemical properties as well as the molecular structures are shown in Table 2 and Fig. 1, respectively. It should be noted that the SRA1 is the commonly used low molecular polyether [7–9] while SRA2 is a novel polymer-type SRA synthesized by unsaturated polyether monomer and acrylic acid through free radical copolymerization and the water-reducing ratio of SRA2 is around 25%.

2.2. Mix proportion

Three groups of cement pastes were prepared in this study (see Table 3). They are plain cement paste and cement pastes with 2.0% dosage (by cement mass) of SRA1 and SRA2, respectively. Small quantities of superplasticizer were added into the plain mixture and SRA1 mixture to obtain a similar workability of the SRA2 mixtures, since SRA2 possesses a function water-reducing. The mixtures were prepared by a planetary mixer and the experiments were conducted at the temperature of 20 ± 2 °C.

2.3. Experimental procedures

2.3.1. Autogenous deformation

The autogenous deformation of early age of the cement pastes were measured by corrugated tubes with length and diameter of 340 mm and 30 mm, respectively. The advantages of this measurement as well as the testing principle can be found in former studies [9,23]. Each of the tubes was sealed on both ends and placed horizontally on a rigid metal frame with one side fixed in the frame. And the non-contact electric eddy transducer was used to measure the displacement of the other end of the tube.

The final set time obtained by Vicat test (ASTM C191) was regarded as the starting point of the deformation of the corrugated tubes [24]. For comparison, the JD18 Universal Projection Length Measuring Instrument was also used to test the autogenous deformation of the mixtures. The sizes of the samples were 25 mm × 25 mm × 280 mm with copper head on both sides of the samples. The samples were demolded at 24 h since the contact of cement and water and covered by the plastic wrap as well as the aluminum foil to prevent the moisture evaporation. Further, the original length was measured immediately after the samples were sealed and then cured at the temperature of 20 ± 3 °C.

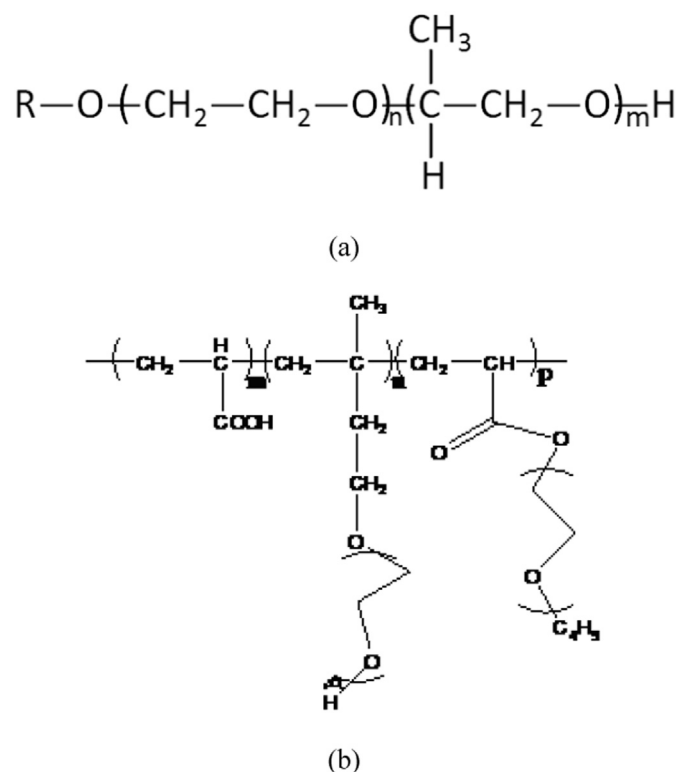


Fig. 1. Molecular structure of the two types of SRA: (a) SRA1; (b) SRA2.

Table 2
Basic physicochemical properties of SRA1 and SRA2.

Name	Solid content (%)	pH	Density (g/cm ³)	Appearance	Type	Average molecular weight (g/mol)
SRA1	≥ 99	10 ± 1	1.00 ± 0.02	Light yellow liquid	Low molecular polyether	2281
SRA2	35	7 ± 1	1.05 ± 0.02	Clear liquid	High-molecular polymer	36,451

Table 3
Mix proportion of the three cement paste mixtures in this study.

Groups	W/C	Superplasticizer (wt%)	SRA (wt%)
Ref	0.30	0.07%	–
SRA1-2.0%	0.30	0.06%	2.0%
SRA2-2.0%	0.30	–	2.0%

2.3.2. Hydration heat

TAM AIR Isothermal calorimeter produced by TA Instruments, Inc. (United States) was used to measure the heat flow and the cumulative heat of the three mixtures under the constant temperature of 20 °C. The cumulative heat release measurement was used to evaluate the evolution of the hydration degree of the cement paste by using the theoretical heat release of complete hydration, which is 430 J/g in this study according to the hydration heat models for cementitious materials [25].

2.3.3. Dynamic elastic modulus

The dynamic elastic modulus was obtained from the ultrasonic wave-speeds values at the age of 1 day, 2 days, 3 days, 7 days and 28 days [26] by using the NM-4B non-metal ultrasonic tester produced by Koncrete Engineering Detection Co., Ltd., while the Poisson's ratio is supposed to be a constant value of 0.22 [9,27].

2.3.4. Internal relative humidity

The internal relative humidity (RH) of the mixtures was measured by the BSS-802 U Dual Channel Temperature-Humidity Recorder produced by Beisheng Gaoke Technology Co., Ltd. (Guangzhou, China). And the testing range of the humidity is 0% to 100% with the standard deviations of 1.1, 0.6 and 0.6 for the plain, SRA1 and SRA2 mixtures respectively (the values were obtained by 2 repetitions for each of the mixtures). The calibration of the RH sensors was performed by putting the RH sensors into the bottles with saturated NaCl, KCl and K₂SO₄ solutions which has the theoretical RH at around 75.5%, 85.1% and 97.6%, respectively [28]. The humidity sensor was imbedded into the hole of the sample (formed by the pre-designed thin PVC pipe barrier inside of each mode) 2 h later after final set of each mixtures and the test interval is 0.5 h.

2.3.5. Pore solution analysis

Pore solution of the cement pastes were obtained by centrifugal machine and high pressure steel die [10,29] for the fresh and harden samples, respectively. The concentration of SRAs were obtained from the total organic carbon measurement (TOC) of the pore solutions using the Multi N/C 3100 Total Organic Carbon Analyzer produced by Analytik Jena AG (Germany) [10]. In order to minimize carbonation, the pore solution was stored in a bottle of 10 ml immediately after extraction and diluted the solutions for 100 times right after they are being collected either from extraction or by centrifuge. Then the solutions were put into a low temperature environment (5 °C) in order to avoid potential reactions and all the tested were done within 24 h at the temperature of 20 ± 0.3 °C. In each experimental stage, no visible precipitation occurs according to the visual observation. The concentrations of K⁺, Na⁺, Ca²⁺ and SO₄²⁻ were obtained by measuring the molar content of the chemical elements K, Na, Ca and S using Inductively Coupled Plasma Optical Emission Spectrometer (ICP-OES)

produced by SPECTRO Analytical Instruments (Germany). Detailed measurement mechanism can be found in former studies [30]. The concentration of OH⁻ was obtained from the pH values of the pore solutions measured by pH needle. It should be noted here that although the tap water is used in this study, the ions concentration in the original mixing water is at least one to two orders of magnitude lower than that of the target ions measured by the ICP-OES, therefore, it is believed that the interference of the ions in the tap water can be neglected.

2.3.6. Content of ettringite and portlandite

The X-ray diffraction (XRD) measurements were conducted to determine the content of the ettringite and portlandite. The preparation procedures of the XRD samples were as follows: (a) 100 ml of each mixture was cast into a plastic bottle and was cured in sealed condition; (b) small pieces of samples were cut at prescribed ages and immersed in isopropanol for 48 h to cease hydration; (c) drying the sample in a vacuum oven for another 48 h at 25 °C and grounded manually through 80 μm square-mesh sieve; (d) 10 wt% corundum was mixed into the powder as the internal standard to fulfill the requirements of the quantification measurement of Rietveld analysis (TOPAS from Bruker AXS was used for the Rietveld refinement) [31]. Finally, the samples were scanned between 5° and 80° in continuous mode with the step size of 0.020° and the scanning speed of 0.3 s/step. And the diffraction data was collected by Bruker D8 Advance X diffractometer in a θ-θ configuration adopting CuKα radiation (λ = 1.54 Å) under a fixed divergence slit size of 0.6°.

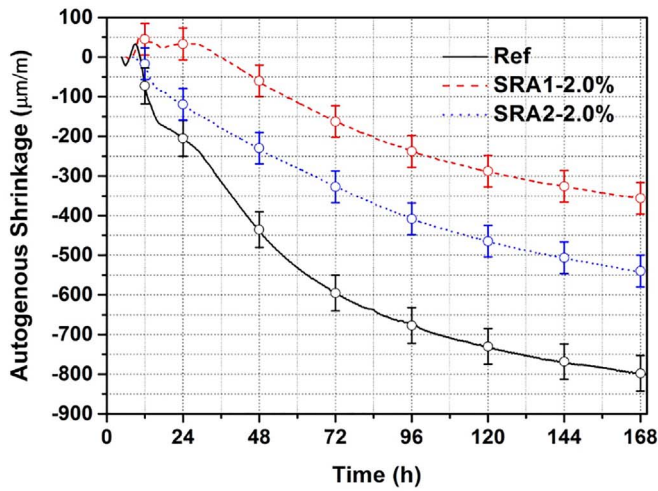
3. Experimental results

3.1. Autogenous shrinkage

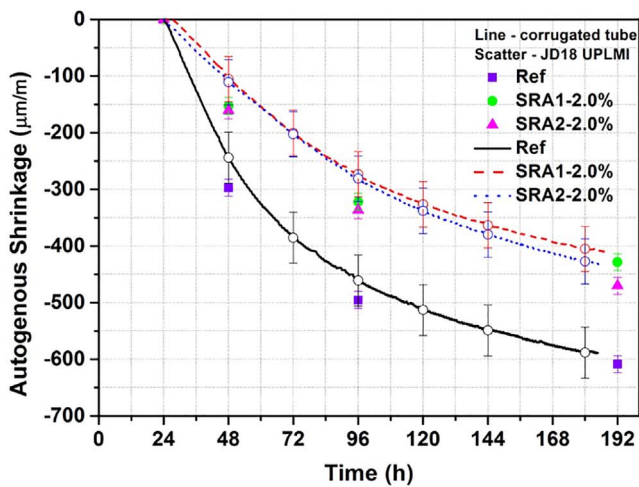
Fig. 2 shows the results of the autogenous deformation of the three mixtures (zeroed to the time of final set and they are 4.7 h, 6 h and 8 h for the plain, SRA1 and SRA2 mixtures, respectively) as a function of time. It should be first noted that the evaluation of the data deviations for each types of the experiments is based on the sample standard deviation of the repetition samples, and the error bars on the curves is calculated according to the results of the repeated samples at the specific ages.

It can be seen in Fig. 2(a) that the autogenous deformations of the samples present different patterns. The plain mixture shows a small degree of expansion comparing with the values measured earlier and soon displays an obvious shrinkage before 72 h. For the SRA1 mixture, the shrinkage curve presents an obvious expansion during the age of 6 h to 28 h, while for the SRA2 mixture, the curve shows no expansive period but a slow rate of shrinkage comparing with the plain mixture.

Fig. 2(b) shows the results of both the methods of corrugated tubes and the length measuring instrument. Since the samples measured by



(a)



(b)

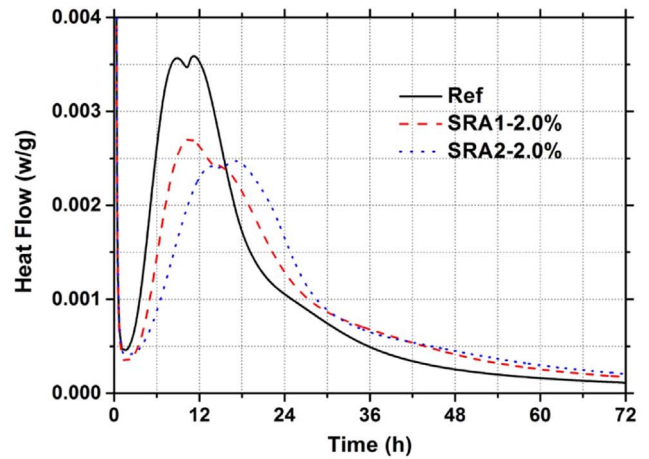
Fig. 2. Autogenous deformations of the cement pastes as a function of time: (a) corrugated tubes zeroed to the time of the final set; (b) comparison of the corrugated polyethylene method and the Universal Projection Length Measuring Instrument zeroed to the time of 24 h.

the second method were demolded at 1 day, the sample lengths at 24 h are treated as the original lengths for both methods. It is obvious that the results of the two types of autogenous deformation measurements were fairly consistent with each other, although a relative small difference between the two methods is observed which is however within the standard deviations of the test results. Meanwhile, the SRA1 mixture and SRA2 mixture possess approximately the same shrinkage-reducing ability after 24 h comparing with the plain mixture.

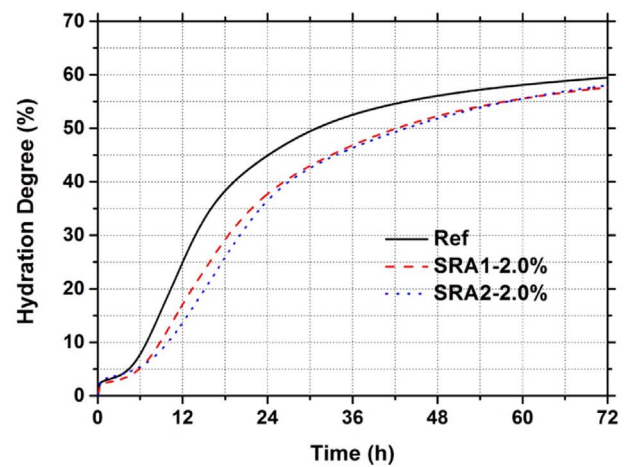
It should be noted that, the addition of 2.0% SRA1 and SRA2 separately into the cement pastes results in a shrinkage reduction of about 33% at 7 days (see Fig. 2(b)). However, when considering the deformation since the final set, the reduction in shrinkage at 7 days is about 55% and 34% for the SRA1 mixture and SRA2 mixture, respectively (see Fig. 2(a)).

3.2. Isothermal conduction calorimetry

Fig. 3 shows the hydration performances of the three mixtures. Similar to previous studies [6,9], both the addition of 2.0% SRA1 and



(a)



(b)

Fig. 3. Hydration performances of the cement pastes as a function of time: (a) heat flow; (b) hydration degree.

SRA2 retard the hydration process and reduce the height of the heat release peak. This phenomenon of the SRA2 mixture is more noticeable than that of the SRA1 mixture (see Fig. 3(a)). In addition, the hydration degree evolutions calculated by the ratio of the cumulative heat release and the theoretically complete heat release are shown in Fig. 3(b) [25]. According to Fig. 3(b), the 24 h hydration degrees of the mixtures containing SRA1 and SRA2 are both 37%, nearly 8% lower than that of the plain mixture while the difference decreases to 4% at the age of 48 h. It is demonstrated by the ICP measurements, which would be shown in the following section, as well as previous studies that the retardation of the cement hydration in the presence of SRAs can be attributed to the reduction of the alkali concentration in the pore solutions and the limitation of the C_3A dissolution at early age [4,9].

3.3. Dynamic elastic modulus

Fig. 4 shows the dynamic elastic modulus evolutions of the mixtures at early age determined by the measurements mentioned in section 2.3.3 and predicted by the CEB-FIP Model (Eq.(3)), [32–33]:

$$E(t_e) = E_{28} \times \{ \exp[s \times (1 - \sqrt{672/(t_e - t_0)})] \}^n \quad (3)$$

where t_e is the equivalent age in standard curing condition which equals to the age of the sample in this study (h); t_0 is the initial set time (h) (they are 3.8 h, 4.8 h and 6 h for the plain, SRA1 and SRA2 mixtures,

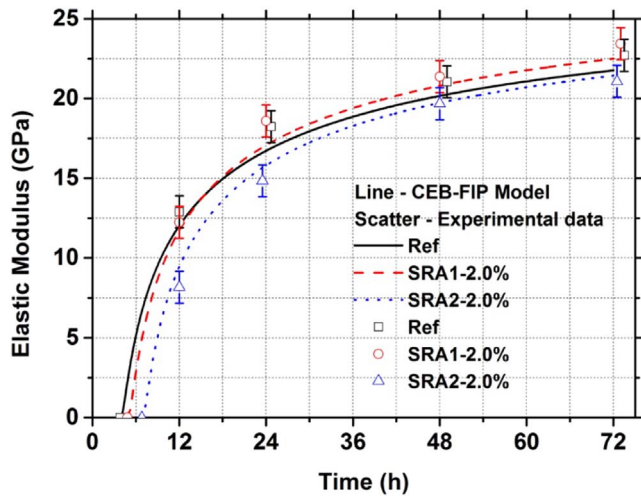


Fig. 4. The measured dynamic elastic modulus of the mixtures and the evolution of dynamic elastic modulus by adopting the CEB-FIP Model at early age.

respectively); E_{28} is the dynamic elastic modulus at 28d (GPa); s and n are constants (0.25 and 0.4 are adopted respectively for the ordinary Portland cement according to [32]).

It can be seen from Fig. 4 that the predicted values agree with the measured data quite well and both of which show a slower development of the dynamic elastic modulus for the SRA2 mixture than that of the other two mixtures due to the later set of the SRA2 mixture, especially before 24 h of hydration, while the dynamic elastic modulus of SRA1 mixture is slightly higher than the plain mixture after the age of 15 h. However, the values of the three mixtures are nearly the same at the age of 28 days, 26.9 GPa, 27.1 GPa and 26.7 GPa for the plain, SRA1 and SRA2 mixtures respectively (not shown in Fig. 4). However, it should be noted that, although the CEB-FIP Model is developed for concrete, it fits well for the results in this study, while any other models also can be used if they capture the experimental results reasonably.

3.4. Internal relative humidity

Fig. 5 shows the internal relative humidity evolution of the sealed samples with and without SRAs as a function of time. It can be seen from Fig. 5 that the internal RH of the plain mixture decreases faster than the mixtures containing SRAs especially during the age of 8 h to 24 h, during which the hydration rate reaches the peak value and the

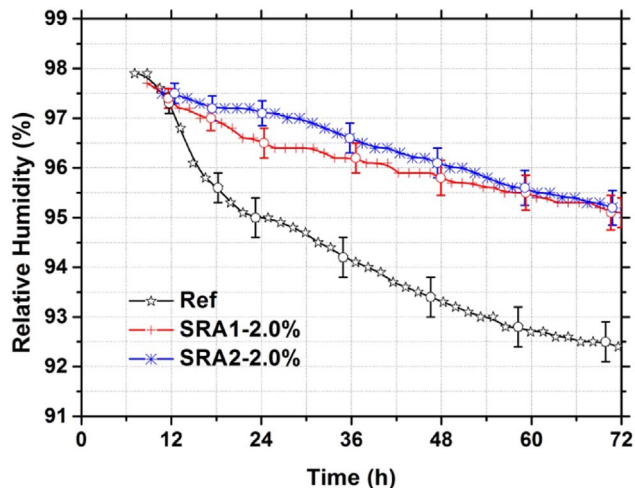


Fig. 5. Internal relative humidity evolutions of the sealed samples with and without SRAs as a function of time.

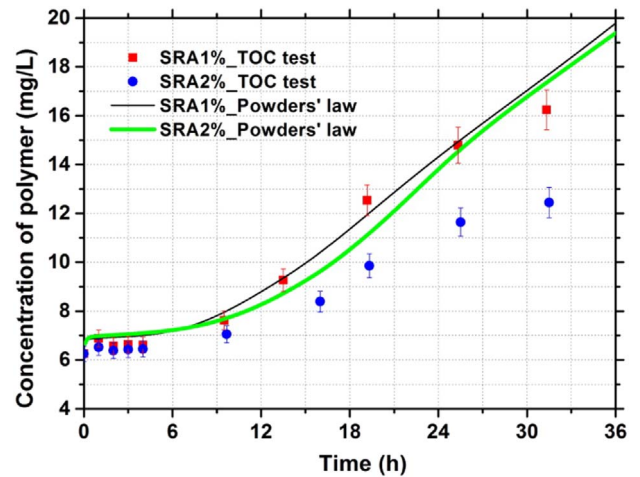


Fig. 6. The concentration of SRA1 and SRA2 in the pore solutions as a function of time.

hydration degree increases dramatically for the plain mixture (see Fig. 3(b)). It can be known that the increasing hydration degree promotes the chemical shrinkage and the consumption of water, resulting in the reduction of the internal RH [1–2,9,17]. However, in the cases of the mixtures containing SRAs, on one hand, the decrease of the surface tension of the pore solutions (see Fig. 6) due to the presence of SRA can reduce the internal equilibrium relative humidity at the same hydration degree according to the Young-Laplace equation (see Eq.(1)) and Kelvin equation (see Eq.(2)), on the other hand, the phenomenon of hydration retardation for SRA mixtures further weaken the potential of the water consumption in turn maintain a relatively higher meniscus radius and higher internal RH according to Eq.(1) and Eq.(2). It should be also noted here that, the measured internal RH of SRA2 mixture presented a higher value than that of SRA1 mixture especially at around 24 h which is mainly because of the lower hydration degree and water consumption at early age. Finally, the internal RH of the SRA1 mixture and SRA2 mixture become nearly the same but also to be 2.5% higher than that of the plain mixture after the age of 48 h.

3.5. Surface tension and SRA concentration

The surface tension of the synthesis pore solutions (prepared by dissolving 0.35 mol/l KOH and 0.05 mol/l NaOH into the deionized water [4]) as a function of SRA concentrations was measured by using the *Sigma 703* surface tension tester according to the authors' former work [34]. As the concentration of SRA1 and SRA2 increase from 0 to 2.0%, the surface tension decreases dramatically from the initial value of 67mN/m to 52mN/m and 56mN/m, respectively. However, further increase of the concentration of SRAs from 2% to 30%, the surface tension of the solution containing SRA1 drops gradually from 52mN/m to 37mN/m while the surface tension of the solution containing SRA2 keeps constantly around 55mN/m.

Fig. 6 shows the concentration of SRA1 and SRA2 in the pore solutions as a function of time. As can be seen in Fig. 6, each of the testing concentrations of SRA1 agrees with the theoretical concentrations of SRA1 calculated by Powers model [35] quite well. While for the SRA2 mixtures, the testing values are all lower than that of the theoretical concentrations as well as the that of the SRA1 mixtures. The lower concentration of SRA2 comparing with SRA1 at the same age after final set is probably due to the obvious adsorption phenomena of SRA2 polymers on the surface of the cement particles as well as the hydration products because of the ionic groups exist in the structure of SRA2 [36]. Meanwhile, the concentrations of the superplasticizer in the pore solution of the plain mixture were also measured which indicates that the amount of the polymers in the plain mixture is small enough to be neglected thus will not influence the test result of the SRA1

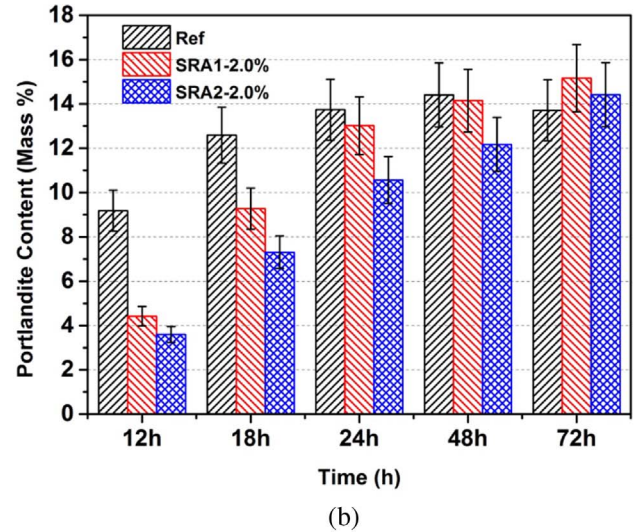
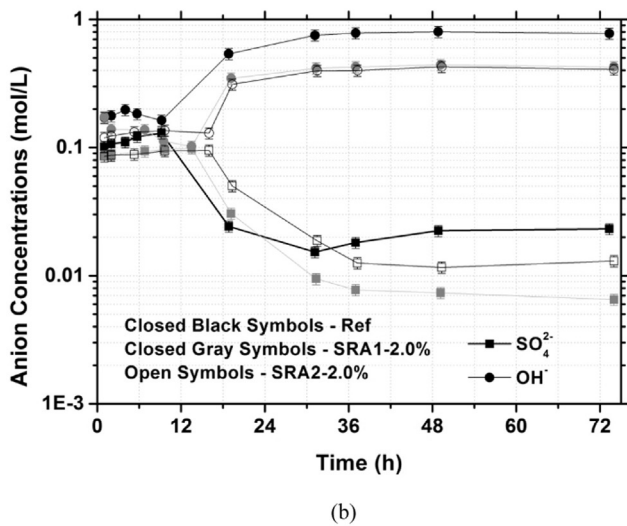
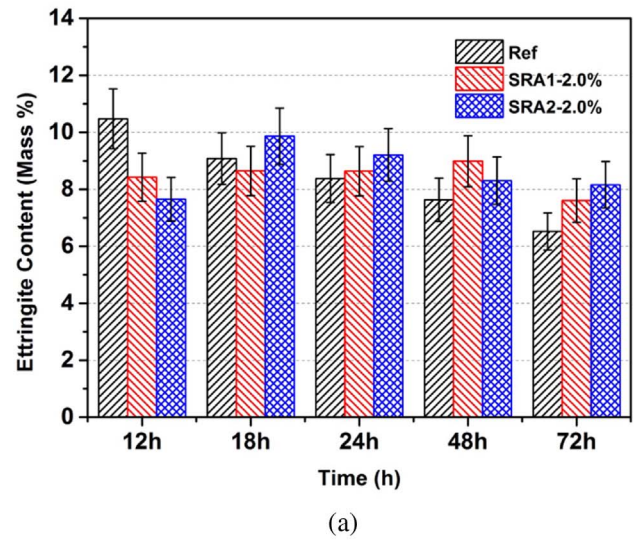
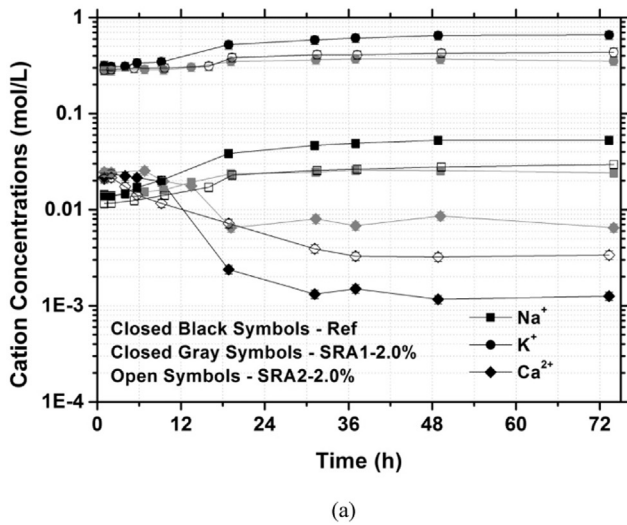


Fig. 7. The concentration of the ions in pore solutions as a function of time: (a) cationic concentrations; (b) anionic concentrations.

Fig. 8. The content of the hydration products over time: (a) ettringite; (b) portlandite.

concentration in the pore solutions.

3.6. Ionic concentrations in pore solutions

Fig. 7 shows the concentration of the cations (K⁺, Na⁺, Ca²⁺) and anions (SO₄²⁻ and OH⁻) in pore solutions as a function of time. It can be seen from Fig. 7 that the concentrations of various ions of the solution containing SRA2 are between that of the plain solution and the SRA1 solution, and are more closer to the solution containing SRA1. The presence of SRA1 and SRA2 both reduce the concentration of the alkali ions (K⁺ and Na⁺) and SO₄²⁻ especially after the critical points mentioned in [4,9], which can be attributed to the reduction of the polarity of the pore solutions due to the presence of the non-polar constituents in the solution [4].

It is also reported that a higher alkali content would cause a lower Ca and higher Al and S concentrations in solution in turn a lower alkali content such as the presence of SRA1 and SRA2 in the cementitious system would lead to a higher Ca and lower S concentrations in solution which is consistent with the results obtained in previous studies [4,9,37].

Moreover, it should be clarified here that the influence of the different pH values between the two SRAs on the alkali content in the pore solution can be ignored. The reason exists in the fact that the pH values

of all the testing ages of the obtained pore solutions are between 13.2–13.9, 13.2–13.6 and 13.1–13.6 for the reference, SRA1 and SRA2 mixtures, respectively, which indicates that the change in the alkalinity due to the dissolution of alkaline ions in the cement clinker is of much higher extents than that of the SRAs' own alkalinity not to mention only 2% of the SRA is added into the mixtures.

3.7. Content of ettringite and portlandite

Fig. 8 shows the content of the ettringite and portlandite before 72 h. It can be seen in Fig. 8(a) that the ettringite generates rapidly and reaches maximum value before 12 h for the plain mixture and drops gradually during 12 h to 72 h. While for the SRA2 mixture, the content of ettringite increases significantly during 12 h to 18 h and drops gradually since then, and the maximum value occurs obviously later than that of plain mixture. For the SRA1 mixture, however, the values at each age situates between plain and SRA2 mixtures then keeps nearly unchanged until 48 h.

It can be known from Fig. 8(b) that the content of portlandite all increase over time from 12 h to 72 h but in different patterns. For the plain mixture, the content of portlandite is relatively high comparing with the other two mixtures and increase obviously during 12 h to 18 h. While for the SRA1 mixture, the content of the portlandite increases

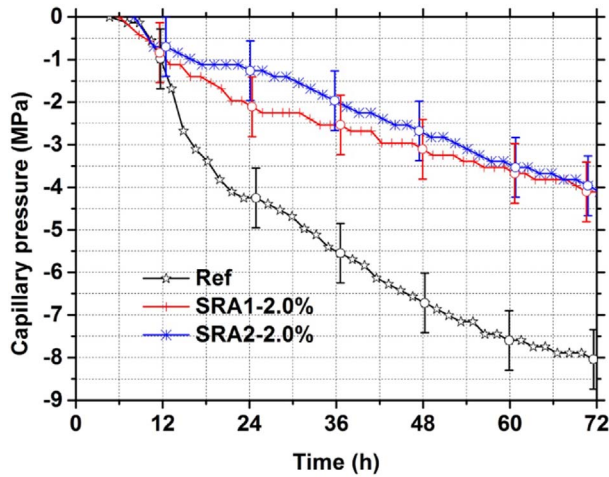


Fig. 9. Simulated capillary pressure evolution of the cement pastes through the measured internal RH as a function of time.

significantly during 12 h to 24 h and is higher than that of the plain mixture at the age of 72 h. For the SRA2 mixture, however, the content of portlandite is obvious lower than the other two mixtures during the testing age.

4. Discussions

4.1. Development of the shrinkage stress

According to Di Bella et al. [38], several models were proposed in order to further interpret the basic mechanisms behind the drying shrinkage and self-desiccation of the cementitious materials. Among those, the Biot-Bishop model (see Eq. (4)) [39–40] gives a good approximation, especially in the case of self-desiccation at high saturation degree [38]. In order to have a better approximation, the modified Biot-Bishop model proposed by Vlahinić et al. [41] is used in this study (Eq. (4)).

$$\epsilon_{auto} = S_w \sigma_{cap} (1/K_b - 1/\bar{K}) / 3 \quad (4)$$

where S_w is the saturation fraction of the cement paste obtained from Powers model [35]; σ_{cap} is the capillary pressure obtained by the RH_k (which due to meniscus formation in the capillary pore, and $RH_k = RH/RH_s$, where RH is the measured values and RH_s is the RH depression due to the presence of ions as and the admixtures and is considered as 98.0%, 96.7% and 96.7% based on the Raoult's law and the results gathered in this study [42]) with the Young-Laplace equation (Eq.(1)) and Kelvin equation (Eq.(2)) which ranges from 0 to 8 MPa and 0–4 MPa for the plain mixture and the SRA mixtures, respectively (Fig. 9); K_b is the time-dependent bulk modulus of the cement paste considering the effects of porosity [9,35] ($K_b = E/3(1 - 2\nu)$, where ν is the Poisson's ratio and a constant value of 0.22 is adopted [9,27]; E is the dynamic elastic modulus and its time-dependent evolution is shown in Fig. 5.); and \bar{K} is the effective bulk modulus which can be calculated as follows:

$$\bar{K} = K_s - (K_s - K_b)(1 - S_w) / (1 - S_w \phi_0) \quad (5)$$

where K_s is the bulk modulus of the solid skeleton (supposing to be 44 GPa according to Lura et al. [35]); ϕ_0 is the total porosity which is calculated by Powers model [35] according to the hydration degree shown in Fig. 3(b).

Based on the related experimental results introduced above, the estimated autogenous shrinkage of the cement pastes are shown in Fig. 10. Similar to the results shown in former study [9], the estimated autogenous deformations of the three mixtures at 72 h are around 110, 55 and 55 microstrains, respectively, which are about 5.5 times, 2.9

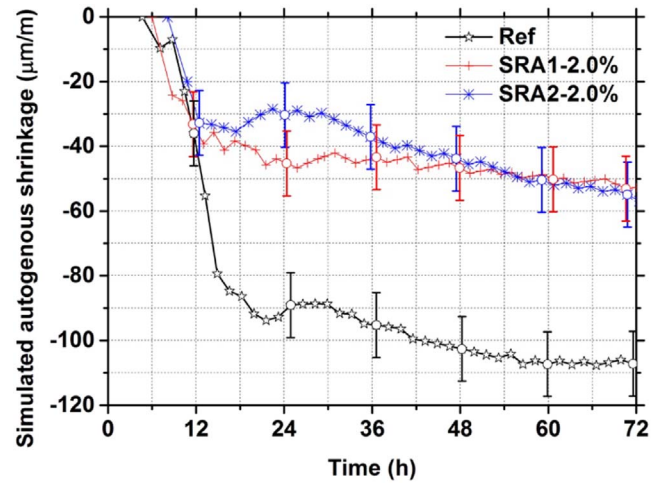


Fig. 10. Simulated autogenous shrinkage of the cement pastes using the Benz model [42–43].

times and 5.9 times lower than the measured autogenous deformations at the same age for the plain mixture and the mixtures containing SRA1 and SRA2, respectively. The discrepancies between the measured and the calculated deformation curves mostly due to the fact that the mixtures show a viscoelastic response to the capillary stresses, of which the authors have only considered the elastic part. Indeed, the pastes would also deform under a sustained internal stress such as the capillary stresses in a manner similar to the creep under external stress [9,43]. However, it is not within the scope of this study.

Further, it is worth noting that although the magnitude of the simulated autogenous deformations do not fit the measured data very well, the calculated deformation curves show obvious gaps between the plain mixture and the mixtures containing SRAs. It is also notable that for the simulated autogenous deformation of the SRA1 mixture, no expansion phenomenon appears during the period of 6 h to 28 h. This is because only internal RH induced capillary pressure is considered in the model which only generate shrinkage stress inside the hardened samples as the decrease of the internal RH [9,35]. Therefore, the model above is only valid for estimating the self-desiccation shrinkage in the mixtures, while for the autogenous deformations which vary non-monotonously, more details need to be considered as follows.

4.2. Development of the expansion stress

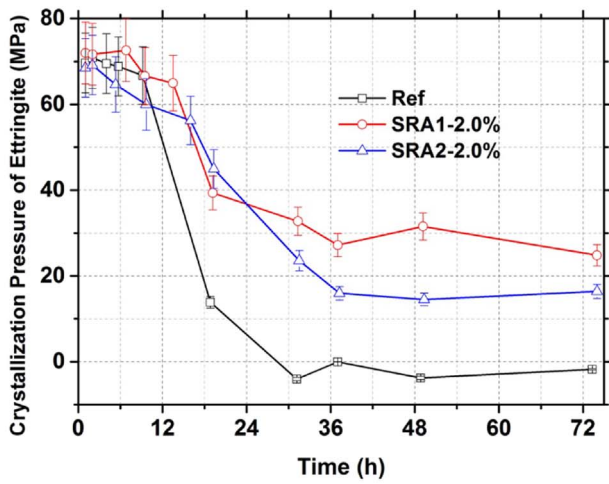
4.2.1. Evolution of the crystallization pressure

It is widely known that with the hydration of cement paste, the formation of the crystalline phases such as ettringite and portlandite will generate the crystallization pressure, while after the final set of the mixture, further development of the crystal will be hindered by the solid structure thus causing a swelling stress [3,9,44–46]. The pressure exerted by the crystal growth on the surface of the solid matrix is given by Eq. (6):

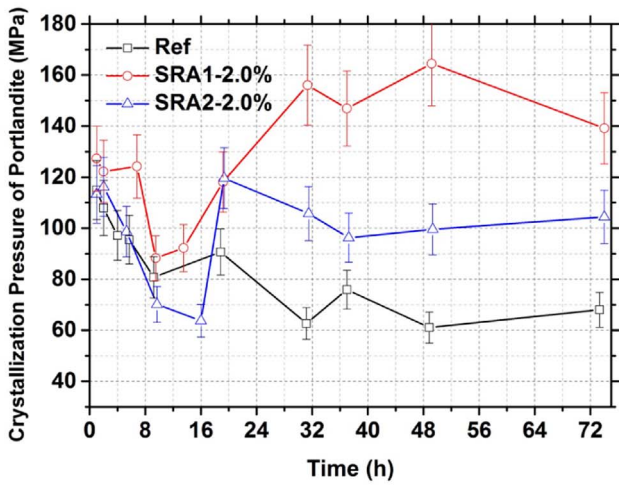
$$\sigma_{cr} = 2\gamma_{CL}/r_{cr} = RT/\gamma_m \cdot \ln(IAP/K_{sp}) \quad (6)$$

where σ_{cr} is the crystallization pressure; γ_{CL} is the crystal/liquid interfacial free energy; r_{cr} is the radius of the crystal growth surface; R is the universal gas constant; T is the absolute temperature; IAP is the ion-activity product of the phase calculated by the thermodynamic software GEMs according to [37] and K_{sp} is the theoretical solubility product of the same phase at equilibrium in aqueous medium (assuming to be water at 298.15 K).

However, in most cases, the swelling stress induced volume expansion of the sealed cementitious materials is offset by the capillary pressure induced shrinkage stress [3]. Nevertheless, recent study shows that the cement paste containing traditional polyether-type SRA would



(a)



(b)

Fig. 11. The calculated crystallization pressure of the crystal phases as a function of time: (a) ettringite; (b) portlandite.

generate a swelling period at the early age of cement hydration [9] which is consistent with the SRA1 mixture studied here. Interestingly, there is no expansive period occurs throughout the deformation development of the SRA2 mixture which will be discussed below.

Fig. 11 shows the crystallization pressure caused by the growth of the ettringite and portlandite as a function of time obtained from the results of the ion concentration evolution (Fig. 7) through Eq. (6) [9]. It can be seen from Fig. 11 that the crystallization pressure of the ettringite is around 70 MPa for all of the three mixtures in the initial stage and present downward trends during the first 24 h. After that, the pressure gradually reduces to a relatively stable value in the cases of the SRA1 mixture (around 30 MPa) and the SRA2 mixture (around 18 MPa), respectively, while there is no crystallization pressure generated by ettringite in the case of the plain mixture.

Nevertheless, the calculated crystallization pressure of the portlandite shows different patterns comparing with that of the ettringite. The values of the SRA1 mixture are always the highest among the three mixtures and the SRA2 mixture ranks the second place after the age of 16 h. It can be known from Fig. 11 that the crystallization pressures generated by portlandite occupies more dominant position comparing with that of the ettringite in general crystallization pressures of all the three mixtures [9].

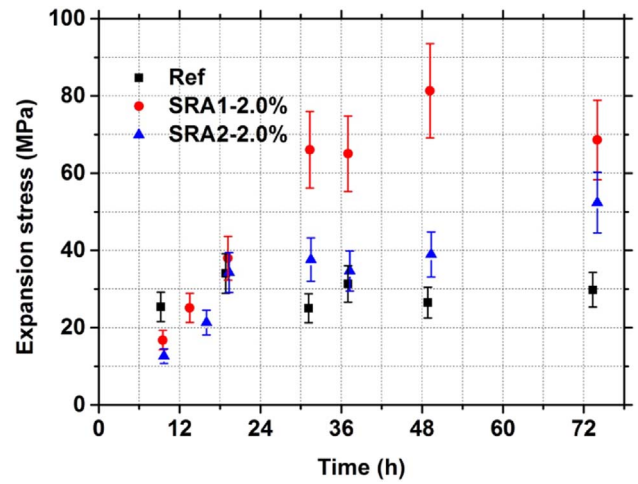


Fig. 12. Simulated expansion stress evolution of the cement pastes as a function of time (without considering the factor R in Eq. (8)).

4.2.2. Evolutions of other pore mechanical parameters

It is worth knowing that besides the crystallization pressure, the volume fraction of the crystal phases in the system, the porosity of the mixture as well as the fraction of the crystal phases that occupying the pores in the system also to be of great importance in determining the expansion stress (Eq. (7)) [44]:

$$\sigma_{exp} = \phi_R \cdot \sigma_{cr} \quad (7)$$

where σ_{exp} is the expansion stress; ϕ_R is the volume fraction of the pore space filled with crystal phases, which can be simplified as Eq. (8) [9]:

$$\phi_R = R \cdot \phi_{cr} / \phi_p \quad (8)$$

where ϕ_{cr} is the volume fraction of the crystal phases in the system; ϕ_p is the porosity of the mixture; R is the fraction of the crystal phases that occupying the pores.

Fig. 12 shows the development of the calculated expansion stress of the three mixtures after final set without considering the factor R in Eq. (8). It can be seen from Fig. 12 that the evolutions of the expansion stress of the two mixtures with SRAs can both be divided into two regimes. For SRA1 mixture, the expansion stress keeps an increasing state until 30 h when the value comes to the plateau of around 70 MPa, while for SRA2 mixture, a relatively slow growth rate of the expansion stress can be observed and the value keeps an obviously lower plateau of around 40 MPa since the age of 20 h. However, in the case of the plain mixture, the value of the expansion stress is the highest among the three mixtures before 12 h (around 25 MPa) and is also keeps nearly unchanged since then.

Importantly, it can be known from Fig. 9 that before the age of 12 h, the shrinkage stress of the three mixtures present similar value while the expansion stress of the plain mixture shows the highest level, which may result in a positive effective stress inside the mixture hence a short period of expansion occurs for the deformation curve of the plain mixture. Similarly, in the case of SRA1 mixture, the continuous growth of the expansion stress during the age of 6 h to 30 h may also offset the gradual growth of the capillary pressure induced shrinkage stress hence a relative longer expansion period occurs for the deformation curve of the SRA1 mixture. However, in the case of the SRA2 mixture, the expansion stress develops rather gradually that it was offset by the shrinkage stress during the whole stage of the deformation hence no expansion period occurs on the deformation curve of SRA2 mixture. Moreover, it should be noted that the expansion stresses of the three mixtures keep nearly unchanged in the second regime (for the plain mixture in this study, it can be confirmed that the first regime exists however it occurs too early to be captured in Fig. 12), while the capillary pressure induced shrinkage stress presents a continuous increase

that the effective stresses all present negative values for the three mixtures which lead to the shrinkage of the hardened mixture at later ages.

4.3. Summary of the shrinkage-reducing mechanisms of SRA1 and SRA2

It is of great interest to analyze the different shrinkage-reducing effects of SRA1 and SRA2 on the deformation behavior of the cement pastes. According to the results obtained above, it is known that the dissolution of the ions are hindered in the SRA mixtures mainly because of the decreased polarity of the pore solution, hence reducing the dissolving capacity of alkali ions which directly influences the hydration process of cement thereby affecting the evolution of the autogenous deformation. However, the cement pastes containing high-molecular polymer-type SRA shows a different pattern of autogenous deformation which is more uniform and monotonous than that of the polyether-type SRA. It can be concluded that the shrinkage-reducing effect of low molecular polyether-type SRA can reduce the surface tension of pore solution significantly thereby maintaining a relatively high internal RH which results in a lower capillary pressure at each hydration period comparing to the plain mixture. In addition, the higher crystallization pressure (mainly induced by the generation of portlandite), the higher content of crystal phases as well as the lower total porosity of the hardened mixture (comparing to that of the SRA2 mixture) have a comprehensive effect of producing a obviously high level of expansion stress which further compensating the shrinkage stress at early age of the cement paste. Differently, the higher extent of adsorption of SRA2 molecule on the surface of solid phase (Fig. 6) regulates the hydration process of cement to a greater extent than that of SRA1 which results in a relatively high internal relative humidity and shows a slightly lower shrinkage stress although the capacity of lowering surface tension is inferior comparing with that of SRA1.

5. Conclusion

This study aimed at investigating the effect of the novel polyether-type SRA on the early age autogenous deformation of the cement pastes as well as comparing the mechanisms with the traditional low molecular polyether-type SRA. Based on the information provided above, the following conclusions can be drawn:

The addition of 2.0% SRA1 and SRA2 separate into the cement pastes with water to cement ratio of 0.3 results in a reduction of about 55% and 34% of the autogenous deformation at the age of 7d, respectively. Besides, an expansive period occurs from 6 h to 28 h for the SRA1 mixture, which contributes to the reducing of the autogenous shrinkage of the cement pastes at early age, while there is no such phenomenon for the SRA2 mixture.

The presence of SRA in the cement pastes regulates the hydration rate and the dynamic elastic modulus at early age, especially for the SRA2 mixture, due to the obvious absorption of SRA2 on the surface of the solid phases which slows down the formation of the micro-structure to a greater extent.

For the SRA1 mixture, the shrinkage-reducing mechanism can be attributed to the synergistic effects of the reducing the surface tension of the pore solutions which decreases the capillary pressure induced shrinkage stress and increases the crystallization pressure induced expansive stress which compensates a part of the shrinkage stress at early age.

Unlike the SRA1, the presence of the SRA2 in the cement paste shows a lower expansive stress than that of the SRA1 mixture and the capacity of reducing the surface tension of the pore solutions is also lower than that of the SRA1. However, the fact of higher hydration regulation effect of SRA2 interpreted by the development of the hydration rate also has an important role on maintaining a relatively high internal RH at early age which results in a significant decrease of the shrinkage stress.

Acknowledgements

The authors gratefully acknowledge the research supports by the National Natural Science Foundation of China (Grant No.: 51225801 and 51438003) and the 973 Program of China (Grant No.: 2015CB655100). And also greatly appreciate Jiangsu Research Institute of Building Science Co., Ltd. and the State Key Laboratory of High Performance Civil Engineering Materials for funding the research project.

Compliance with ethical standards

Conflict of interest

The authors declare that they have no conflict of interest.

References

- [1] O.M. Jensen, P.F. Hansen, Autogenous deformation and change of the relative humidity in silica fume-modified cement paste, *ACI Mater. J.* 93 (6) (1996) 539–543.
- [2] O.M. Jensen, P.F. Hansen, Autogenous deformation and RH-change in perspective, *Cem. Concr. Res.* 31 (12) (2001) 1859–1865.
- [3] K. Kovler, S. Zhutovsky, Overview and future trends of shrinkage research, *Mater. Struct.* 39 (9) (2006) 827–847.
- [4] F. Rajabipour, G. Sant, J. Weiss, Interactions between shrinkage reducing admixtures (SRA) and cement paste's pore solution, *Cem. Concr. Res.* 38 (5) (2008) 606–615.
- [5] W. Sun, C. Miao, *Theory and Techniques of Modern Concrete*, Science, Beijing, (2012), pp. 161–267 (In Chinese).
- [6] K.J. Folliard, N.S. Berke, Properties of high-performance concrete containing shrinkage-reducing admixture, *Cem. Concr. Res.* 27 (9) (1997) 1357–1364.
- [7] D.P. Bentz, Influence of shrinkage-reducing admixtures on early-age properties of cement pastes, *J. Adv. Concr. Technol.* 4 (3) (2006) 423–429.
- [8] B. Rongbing, S. Jian, Synthesis and evaluation of shrinkage-reducing admixture for cementitious materials, *Cem. Concr. Res.* 35 (3) (2005) 445–448.
- [9] G. Sant, B. Lothenbach, P. Juilland, et al., The origin of early age expansions induced in cementitious materials containing shrinkage reducing admixtures, *Cem. Concr. Res.* 41 (3) (2011) 218–229.
- [10] Q. Ran, N. Gao, J. Liu, et al., Shrinkage action mechanism of shrinkage-reducing admixtures based on the pore solution, *Mag. Concr. Res.* 65 (18) (2013) 1092–1100.
- [11] P. Lura, B. Pease, G.B. Mazzotta, et al., Influence of shrinkage-reducing admixtures on development of plastic shrinkage cracks, *ACI Mater. J.* 104 (2) (2007) 187–194.
- [12] J. Mora-Ruacho, R. Gettu, A. Aguado, Influence of shrinkage-reducing admixtures on the reduction of plastic shrinkage cracking in concrete, *Cem. Concr. Res.* 39 (3) (2009) 141–146.
- [13] J. Saliba, E. Rozière, F. Grondin, et al., Influence of shrinkage-reducing admixtures on plastic and long-term shrinkage, *Cem. Concr. Compos.* 33 (2) (2011) 209–217.
- [14] D. Bentz, M. Geiker, K. Hansen, Shrinkage reducing admixtures and early-age desiccation in cement pastes and mortars, *Cem. Concr. Res.* 31 (7) (2001) 1075–1085.
- [15] M.S. Meddah, M. Suzuki, R. Sato, Influence of a combination of expansive and shrinkage-reducing admixture on autogenous deformation and self-stress of silica fume high-performance concrete, *Constr. Build. Mater.* 25 (1) (2011) 239–250.
- [16] A.B. Ribeiro, A. Goncalves, A. Carrajola, Effect of shrinkage reducing admixtures on the pore structure properties of mortars, *Mater. Struct.* 39 (2) (2006) 179–187.
- [17] J. Weiss, P. Lura, F. Rajabipour, et al., Performance of shrinkage-reducing admixtures at different humidities and at early ages, *ACI Mater. J.* 105 (5) (2008) 478–486.
- [18] G. Sant, F. Rajabipour, P. Lura, W.J. Weiss, Examining time-zero and early age expansion in pastes containing shrinkage reducing admixtures (SRAs), 2nd International RILEM Symposium on Advances in Concrete through Science and Engineering, RILEM, Quebec City, Canada, 2006 (p. 353).
- [19] T. Sugiyama, A. Ohta, Y. Tanaka, et al., Shrinkage reducing type of advanced superplasticizer, Proceeding Fourth Canada Centre for Mineral and Energy Technology: American Concrete Institute/Japan Concrete Institute International Conference on Recent Advances in Concrete Technology, 1998, pp. 189–200.
- [20] T. Sugamata, T. Kinoshita, M. Yaguchi, et al., Characteristics of concrete containing a shrinkage-reducing superplasticizer for ultra-high-strength concrete, 8th CANMET/ACI International Conference on Superplasticizer and other Chemical Admixtures in Concrete, 2006, pp. 51–66.
- [21] H. Nakanishi, S. Tamaki, Performance of multi-functional and multipurpose superplasticizer of new generation in concrete, 7th CANMET/ACI International Conference on Superplasticizers and Other Chemical Admixtures, 2003, pp. 327–342.
- [22] Q. Ran, C. Miao, J. Liu, et al., Performance and mechanism of a multi-functional superplasticizer for concrete, *Mater. Trans.* 47 (6) (2006) 1599–1604.
- [23] O.M. Jensen, P.F. Hansen, A dilatometer for measuring autogenous deformation in hardening portland cement paste, *Mater. Struct.* 28 (1995) 181.
- [24] M. Wyrzykowski, Z. Hu, S. Ghourchian, et al., Corrugated tube protocol for autogenous shrinkage measurements – review and statistical assessment, *Mater. Struct.*

- 50 (1) (2017) 57.
- [25] A.K. Schindler, K.J. Folliard, Heat of hydration models for cementitious materials, *ACI Mater. J.* 102 (1) (2005) 24–33.
- [26] M. Jiang, J. Chen, D. Yang, Dynamic modulus of cement mortar in sulphate erosion measured by ultrasonic checking, *J. Chin. Ceram. Soc.* 33 (1) (2005) 126–132 (In Chinese).
- [27] G. Sant, M. Dehadrai, D. Bentz, et al., Detecting the fluid-to-solid transition in cement pastes, *Concr. Int.* 31 (6) (2009) 53–58.
- [28] Z. Wang, Y. Zhou, S. Li, et al., *Physical Chemistry*, 4th ed., Higher Education, Beijing, 2001 (In Chinese).
- [29] L.J. Buckley, M.A. Carter, M.A. Wilson, et al., Methods of obtaining pore solution from cement pastes and mortars for chloride analysis, *Cem. Concr. Res.* 37 (11) (2007) 1544–1550.
- [30] W. Li, X. Zhu, J. Hong, et al., Effect of anionic emulsifier on cement hydration and its interaction mechanism, *Constr. Build. Mater.* 93 (2015) 1003–1011.
- [31] K.L. Scrivener, T. Füllmann, E. Gallucci, et al., Quantitative study of Portland cement hydration by X-ray diffraction/Rietveld analysis and independent methods, *Cem. Concr. Res.* 34 (9) (2004) 1541–1547.
- [32] CEB Bulletin, CEB-FIP Model Code, London, British Standard Institution, Vol. 1993 (1990).
- [33] X. Zhu, Crack-resistant mechanism of expansive abrasion-resistant concrete under simulated in-situ temperature history and constraint, PhD Thesis, Nanjing Hydraulic Research Institute, 2015 (In Chinese).
- [34] W. Zuo, Q. Tian, Q. Ran, et al., Properties and mechanism of shrinkage reducing admixtures (SRA) in concrete, *Journal of building materials* 19 (2016) 504–510 (In Chinese).
- [35] P. Lura, O.M. Jensen, K. van Breugel, Autogenous shrinkage in high-performance cement paste: an evaluation of basic mechanisms, *Cem. Concr. Res.* 33 (2) (2003) 223–232.
- [36] P.K. Mehta, P.J.M. Monteiro, *Concrete Microstructure, Properties, and Materials*, The McGraw-Hill Companies, Inc., New York, 1993, pp. 281–295.
- [37] P. Feng, C. Miao, J.W. Bullard, Factors influencing the stability of AFm and Aft in the Ca–Al–S–O–H system at 25 °C, *J. Am. Ceram. Soc.* 99 (3) (2015) 1031–1041.
- [38] C. Di Bella, M. Wyrzykowski, P. Lura, Evaluation of the ultimate drying shrinkage of cement-based mortars with poroelastic models, *Mater. Struct.* 50 (1) (2017) 52.
- [39] M.A. Biot, M.A. Blot, General theory of three dimensional consolidation general theory of three-dimensional consolidation, *J. Appl. Phys.* 12 (2) (1941) 155–164.
- [40] A.W. Bishop, G.E. Blight, Some aspects of effective stress in saturated and partly saturated soils, *Géotechnique*. 13 (1963) 177–197.
- [41] I. Vlahinić, H.M. Jennings, J.J. Thomas, A constitutive model for drying of a partially saturated porous material, *Mech. Mater.* 41 (3) (2009) 319–328.
- [42] H. Chen, M. Wyrzykowski, K. Scrivener, P. Lura, Prediction of self-desiccation in low water-to-cement ratio pastes based on pore structure evolution, *Cem. Concr. Res.* 49 (2013) 38–47.
- [43] M. Wyrzykowski, P. Lura, F. Pesavento, D. Gawin, Modeling of internal curing in maturing mortar, *Cem. Concr. Res.* 41 (2011) 1349–1356.
- [44] Z. Sun, G.W. Scherer, Effect of air voids on salt scaling and internal freezing, *Cem. Concr. Res.* 40 (2) (2010) 260–270.
- [45] G.W. Scherer, Crystallization in pores, *Cem. Concr. Res.* 29 (1999) 1347–1358.
- [46] G.W. Scherer, Stress from crystallization of salt, *Cem. Concr. Res.* 34 (2004) 1613–1624.